Chemical Science

ROYAL SOCIETY OF CHEMISTRY

REVIEW

View Article Online
View Journal | View Issue

Cite this: *Chem. Sci.*, 2022, **13**, 9468

Bioimaging agents based on redox-active transition metal complexes

Shan-Shan Xue, † Yingbo Pan,† Wei Pan, Shujie Liu, Na Li * and Bo Tang *

Received 9th May 2022
Accepted 27th July 2022

DOI: 10.1039/d2sc02587f

rsc.li/chemical-science

Detecting the fluctuation and distribution of various bioactive species in biological systems is of great importance in determining diseases at their early stages. Metal complex-based probes have attracted considerable attention in bioimaging applications owing to their unique advantages, such as high luminescence, good photostability, large Stokes shifts, low toxicity, and good biocompatibility. In this review, we summarized the development of redox-active transition metal complex-based probes in recent five years with the metal ions of iron, manganese, and copper, which play essential roles in life and can avoid the introduction of exogenous metals into biological systems. The designing principles that afford these complexes with optical or magnetic resonance (MR) imaging properties are elucidated. The applications of the complexes for bioimaging applications of different bioactive species are demonstrated. The current challenges and potential future directions of these probes for applications in biological systems are also discussed.

1. Introduction

The homeostasis of bioactive species plays a vital role in determining the physiological and pathological states of living systems.[1,2] The fluctuation and distribution of bioactive species are various for different cells at different states, while many diseases, such as cancer and neurological diseases, are closely related to the abnormal fluctuation and distribution of these bioactive species.[3–6] Therefore, selective and accurate detection of these species holds tremendous promise for accurate diagnosis and treatment of diseases. A lot of probes have been developed in the past few decades using different imaging modalities including optical imaging (OI),[7,8] magnetic resonance imaging (MRI),[9–11] X-ray computed tomography (CT),[12,13] positron emission tomography (PET),[14] *etc.* Metal complex-based bioimaging agents have attracted extensive attention due to their properties of low toxicity and good biocompatibility, as well as rich and stable photophysical and electromagnetic properties.[9,15–18]

Transition metal complexes usually consist of one or more metal ions and some organic molecules as ligands. By changing the metals and ligands, the geometric structures and properties of complexes will be various.[19–21] Therefore, different functions of complexes could be realized by modifying their metal ions or ligand structures. Some metal complexes essential for life are commonly used as catalytic centers in metalloenzymes. The biomimetic studies using metal complexes as biologically relevant catalysts have been inspiring.[22–27] These biologically relevant transition metals, including iron, manganese, zinc, and copper, can bind with different ligands to form complexes with the properties of catalytic reactivities and good fluorescence.[7,20,28–30] The application of the metals essential for life can avoid the introduction of exogenous metals and the problems of biotoxicity and metabolism.[31,32] In recent years, a series of metal complex-based probes have been developed with OI and MRI modalities, which can overcome the shortages of organic molecular probes and avoid the metabolic difficulty and biotoxicity of nano-sized probes.[9,16,19] More importantly, metal complex-based probes have the potential to be used as bioimaging agents in clinics. Developing more efficient probes for bioimaging applications based on these biologically relevant metal complexes is very desirable.

Recently, some excellent reviews on metal complex-based molecular probes have been published from different perspectives, such as various optical properties determined by electronic configurations,[19] targeting design for biomolecules,[15,33] imaging and therapeutic bifunctionality for specific diseases,[18] responsive lanthanide luminescence,[34] and functionalization with dendrimers.[17] This review will focus on summarizing the research progress of redox-active metal (iron, manganese, and copper) complexes, which play essential roles in life, as bioimaging agents for both optical and MR images in recent five years. The review will be divided into four parts: the introduction about this topic, the designing principles of metal complex-based probes, the metal complexes used for bioimaging, and conclusion and perspectives for further development.

College of Chemistry, Chemical Engineering and Materials Science, Key Laboratory of Molecular and Nano Probes, Ministry of Education, Collaborative Innovation Centre of Functionalized Probes for Chemical Imaging in Universities of Shandong, Institute of Molecular and Nano Science, Shandong Normal University, Jinan, 250014, P. R. China. E-mail: lina@sdnu.edu.cn; tangb@sdnu.edu.cn

† These authors contributed equally to this work.

2. Designing principles of transition metal complex-based probes

Metal complexes are mainly constructed from two functional units, metal ions and ligands. As a result, the molecular probes based on metal complexes could be achieved by recognizing and reacting the targets using metal ions or ligands. The redox-active transition metal complexes discussed in this review are based on Fe, Mn, and Cu, which are redox-active transition metal ions with rich valent states. The ligands of these complexes are usually poly- or macrocyclic pyridine and porphyrin derivatives, using 4 to 8 nitrogen (N) and oxygen (O) atoms as coordination sites to bind with the metal ions.[35,36] The configurations and properties of complexes could be varied by changing the ligands, even using the same metal ion as the coordination center. Through reacting with the targets, the metal valence or ligand will change, and the fluorescent or magnetic signals will show up.[16] The OI or MRI or dual modalities of these probes in detecting the bioactive species in biological systems could be selected according to their property changes.

OI is one of the most widely used imaging techniques to monitor the physiological and pathological processes in biological systems owing to the advantages of high resolution, good sensitivity, and low cost.[19,37–39] Roughly speaking, the complexes will form new energy level structures, such as highest occupied molecular orbitals (HOMOs) or lowest unoccupied molecular orbitals (LUMOs), which makes the electron transfer between the energy levels much easier and quantum yield higher for complexes than that of the ligands.[40,41] The luminescence mechanisms of complexes mainly include intramolecular ligand charge transfer (ILCT), ligand-to-metal charge transfer (LMCT), metal-to-ligand charge transfer (MLCT), and ligand-to-ligand charge transfer (LLCT).[40,42,43] The complexes could be utilized as OI agents when the excited states of the target-reacted species could be generated through each one of these mechanisms.[44] For the Fe and Mn complex-based probes, OI usually could be achieved from the outstanding optical properties of inherent excited states using appropriate polypyridine and porphyrin derivatives as ligands, or by connecting an organic fluorophore (not participating in coordination) to the ligand.[45] Cu complexes with tetrahedral configuration are commonly used as OI agents, while some examples are also reported using a fluorophore as ligand, through oxidizing or reducing the Cu valence, and de-metallization of the fluorophore and the optical properties will obviously change.[46,47]

MRI is another widely used noninvasive diagnostic imaging technique, which can generate high resolution images through excitation of nucleus using long wavelength radio frequency.[9] For the paramagnetic metal ions, the complexes could be utilized as MRI contrast agents (CAs). The redox-active transition metal ions discussed in this review can change their valence to result in the paramagnetic to antimagnetic property changes through reacting with the active species. Some Fe and Mn complexes have been reported as MRI CAs through the metal magnetic property changes, to detect oxidative bioactive species (*e.g.*, H_2O_2) efficiently.[48–50] Besides, several MRI-based techniques have been developed, including proton (^{1}H) MRI, ^{19}F MRI, and chemical exchange saturation transfer (CEST).[51] ^{1}H MRI is the most commonly used, which could provide clear images of tissues due to the abundance of protons in the body. ^{19}F MRI and CEST have attracted growing interest, and some examples have been published using metal complexes. ^{19}F MRI uses F for quantitative analysis,[52] and the ^{19}F signal could be enhanced by the paramagnetic metals through reducing longitudinal relaxation times (T_1), resulting in more efficient images.[53] Therefore, complexes with proper F containing ligands and paramagnetic metal ions could be used as efficient ^{19}F MRI agents. The MRI modality using the CEST mechanism works through irradiation of protons that can exchange with bulk H_2O.[54] The magnetization transfer results in the signal decrease of the bulk H_2O.[55,56] The CEST signal has inherent sensitivity towards pH, which makes the modality suitable for accurately detecting pH values *in vivo*.[56] For the paramagnetic metals, the oxidation potentials of the complexes are usually lower than the reduction potentials of the bioactive targets, which makes the redox reactions happen and the magnetic properties of complexes change. For the other three magnetic techniques, Fe and Mn complexes usually use macrocyclic ligands, while Cu complexes are four-coordinated with aliphatic ligands. With the increasing research interest, the OI and MRI using metal complexes can potentially offer an attractive solution to the unmet clinical applications in detecting diseases.

3. Metal complexes in bioimaging application

3.1 Iron complexes

Iron is one of the most important essential trace metals for life.[57] Biological systems utilize iron in numerous vital biochemical processes, including oxygen transport, DNA replication, and various redox reactions, owing to its capacity of electron transfer and cycling between different oxidation states.[58,59] Iron complexes are required as a catalytic center for many redox enzymes, such as cytochrome P450, to mediate many redox processes that are crucial for energy production and intermediate metabolism.[60] In recent years, the applications of iron complexes as sensors have been widely studied due to their rich valence state changes and excellent photomagnetic properties, especially for optical and MR imaging. The structures of Fe complex-based probes summarized in this review are shown in Fig. 1. The properties of these agents have been summarized in Table 1.

3.1.1 Iron complexes as regular MRI agents. Iron complex-based probes have been commonly used in magnetic resonance imaging (MRI) studies, some of which have been developed for detection *in vivo*.[61–68] For the regular MRI studies, the trivalent state of Fe(III) complexes is expected to remain in the biological environment. The Fe(III) ion could be stabilized in solution by changing the structures of ligands to make the Fe(III)/Fe(II) redox potentials low enough. Morrow's group reported a series of Fe(III) macrocyclic complexes as MRI agents.[66,67,69–71] For

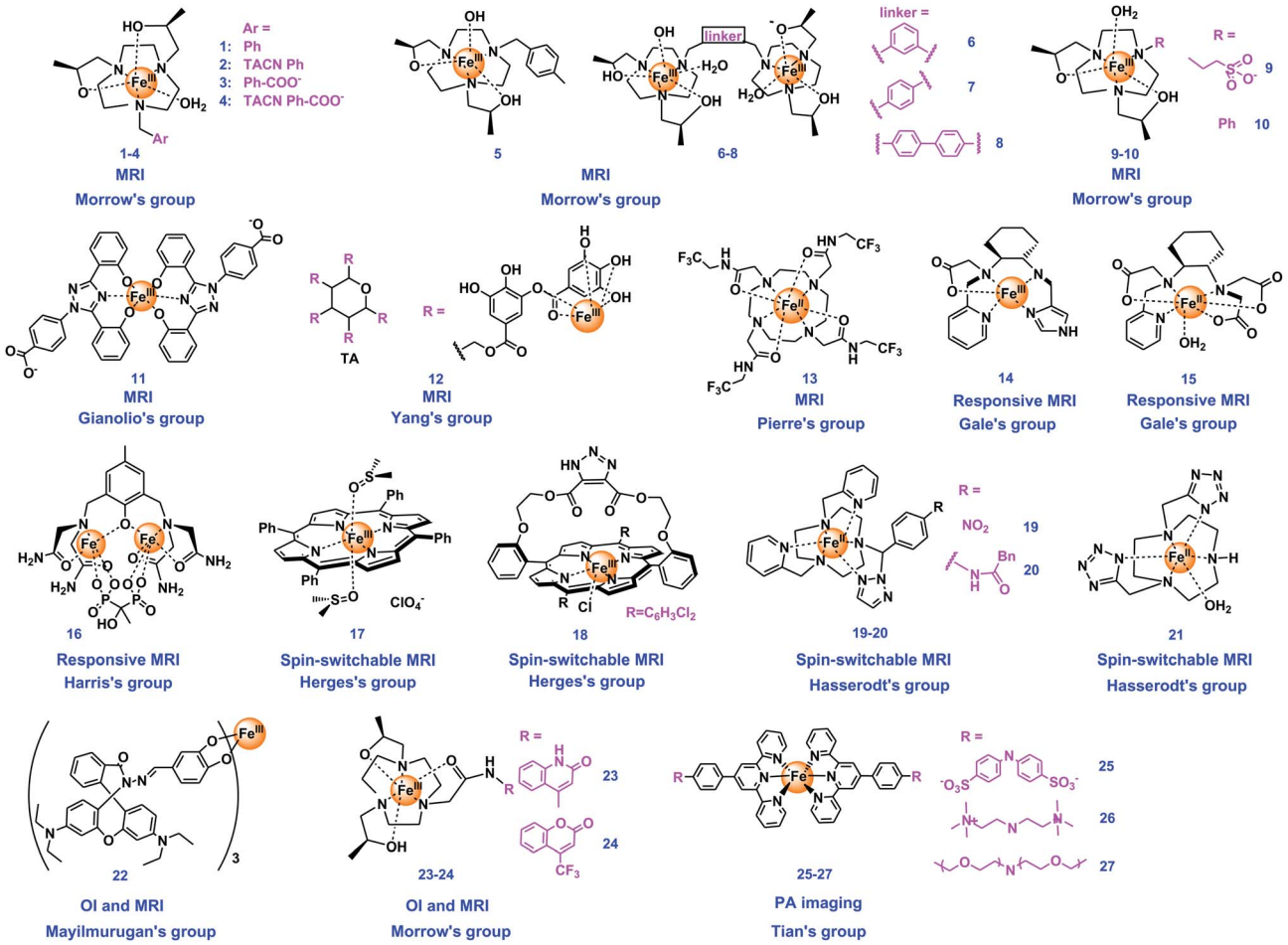

Fig. 1 Chemical structures of iron complexes used as bioimaging agents.

example, they constructed four Fe(III) macrocyclic complexes (**1–4**, Fig. 1) with alcohol donor groups as effective T_1 MRI CAs. **1–4** were prepared from Fe(II) salts, while stabilized high-spin Fe(III) showed small redox potentials of less than −200 mV in neutral solution. The high r_1 relaxivity values of these Fe(III) complexes lacking a rapidly exchanging inner-sphere water, are likely from the strong second-sphere interactions of water mediated by alcohol or hydroxide ligands or by a hydrogen bonding network. The T_1 relaxivity of **1** in serum phantoms at 4.7 T is similar to that of the clinically used Gd(III) agent. **1** shows enhanced kidney specificity in mice MRI studies, and produces an enhancement in T_1 relaxation rates 30 min after injection. The value in kidney is higher than the clinically used Gd(III) and would be further developed as T_1 MRI CA.[66] They also prepared four high-spin Fe(III) macrocyclic complexes from Fe(II) salts and ligands (**5–8**, Fig. 1), including three binuclear complexes and one mononuclear complex, as MRI probes. Water proton T_1 relaxation times of inner-sphere interactions with Fe(III) ions indicated that diiron complexes are much more effective than the mononuclear complex, among which the dinuclear complex with macrocycles linked through *para*-substitution of an aryl group (**7**, Fig. 1) showed the most effective MRI properties, enhanced r_1 for per iron center of blood pool and renal contrast in mice MRI studies.[64] They presented another two new Fe(III) complexes (**9** and **10**, Fig. 1) as stable CAs, with the electrode potentials too negative for redox cycling of Fe(III) to Fe(II). Through appending the sulfonate or hydroxyl groups of the ligands, the MRI properties of the two complexes showed major differences. r_1 relaxivity in this system comes from second-sphere water interaction with the Fe(III) center. **9** showed excellent solubility, low plasma protein binding, and strong r_1 relaxivity, and is expected to be developed as an extracellular fluid CA.[71]

Gianolio's group also designed an Fe(III)-based MRI T_1 CA (**11**, Fig. 1). **11** possesses an excellent thermodynamic stability, a high binding affinity with human serum albumin that three complex molecules can bind to protein at the same time, and a good relaxivity that increases in the range of 20–80 MHz. The reason for relaxation enhancement was revealed that the second sphere water molecules probably formed hydrogen bonds with the coordinating phenol-oxygen, while further enhancement was observed by binding albumin to form the supramolecular adduct. The contrast ability of **11** was comparable to that of the commercial agent Gd^{III} (DTPA). Furthermore, the complex could be completely removed within 24 h from blood samples of healthy mice, which can avoid the issues brought by exogenous Gd. In this work, the Fe(III) center of **11** is highly robust to any redox, and the reduction of **11** to Fe(II) species is not anticipated

Table 1 Iron complexes as bioimaging agents

Imaging agents	Type of agents	Contrast/fluorescence enhancement	Magnetic field	Relaxivity (mM^{-1} s^{-1})	Detection mechanisms	Targets	Ref
1–4	MRI	Δr_1 of **1** was 6-fold higher in the kidney than for Gd(DTPA) at 30 minutes	4.7 T, 37 °C	**1**: $r_1 = 3.8$, $r_2 = 6.2$, **3**: $r_1 = 1.8$, $r_2 = 3.0$	Proton relaxivity of water from second-sphere interactions with Fe	Kidney image	66
5–8		The most effective **7** increased 3-fold in r_1 relaxivity compared to **5**	4.7 T, 37 °C	**5**: $r_1 = 1.83$, **6**: $r_1 = 4.06$, **7**: $r_1 = 5.26$, **8**: $r_1 = 4.36$	Proton relaxivity of inner-sphere water exchange	Blood pool and kidney	64
9, 10		Enhanced bladder and kidney contrast	4.7 T, 37 °C	**9**: $r_1 = 2.0$, **10**: $r_1 = 0.97$	Proton relaxivity of water from second-sphere interactions	Kidney image	71
11	MRI	$\Delta r_1 = 1.4$ mM^{-1} s^{-1} with HSA	0.47 T, 37 °C	**11**: $r_1 = 1.7$, **11**/HSA: $r_1 = 3.1$	Proton relaxivity, second sphere water molecules; binding BSA	Human serum albumin (BSA); cancer	65
12	MRI	Significant increase	1 T	**12**/HSA: $r_1 = 3.47$	Inner-sphere water proton relaxivity; binding BSA	*In vivo* imaging and PTT	72
13	^{19}F and CEST dual modal MRI	CEST signal increase between pH 6.9 and 7.4; ^{19}F independent of pH	—	Detection limitation: 2 mM	^{19}F and CEST MRI signals at different pH	*In vivo* pH mapping	73
14	pH-responsive MRI	$\Delta r_1 = 1.56$ mM^{-1} s^{-1}, over 7-fold increase	4.7 T, 37 °C	Dimer: $r_1 = 0.14$ monomer: $r_1 = 1.7$	Proton relaxivity, deprotonation of the dimer forms the high-relaxivity monomeric complex	pH changes	74
15	L-Cys, H_2O_2 responsive MRI	10- to 15-fold increase	4.7 T, 37 °C	Fe(II): $r_1 = 0.18$, Fe(III): $r_1 = 2.4$	H_2O_2 rapidly oxidizes **14** from Fe(II) to Fe(III), resulting in higher relaxivity	L-Cys, H_2O_2 pathological change *in vivo*	48
16	Redox-dependent PARACEST MRI	—	9.4 T	—	Redox-dependent PARACEST	Ratiometric quantitation of the redox environment	49
17	Spin switchable MRI	$\Delta r_1 = 10.0$ mM^{-1} s^{-1}, over 15-fold increase	—	High spin: $r_1 = 10.6$, low spin: $r_1 = 0.6$	Light-controlled spin switching; inner sphere water proton relaxation	High-spin catalytic species generation of artificial enzyme systems	75
18		—	—	—	Light switching of deprotonated and photodissociable ligand bound high-spin Fe(III)	pH responsive CA	76
19, 20		T_1 decrease of 80–90%	11.4 T, 37 °C	—	Analyte switched high-spin Fe(II), inner sphere water proton relaxation	Catalytic hydrogenation and penicillin amidase	78
21		—	7 T	$r_1 = 0.57$	Analyte switched high-spin Fe(II), inner sphere water proton relaxation	A specific targeted enzyme	79
22	OI–MRI dual modal	r_1 relaxivity significantly enhanced	—	—	Rhodamine catecholate and inner sphere water proton relaxation	NO and acidic pH	80
23, 24		—	4.7 T, 37 °C	+HSA: **23**: $r_1 = 1.10$, **24**: $r_1 = 1.06$	Second-sphere water proton relaxation	Yeast cells	67
25–27	PA imaging	—	—	—	Photoacoustic signal	Multi-modal imaging	81

under physiological conditions.[65] Yang's group developed a strategy to develop a nontoxic Fe(III) complex, constructed by using tannic acid (TA), a large natural polyphenol, and bovine serum albumin (BSA), **12**@BSA, which slows the molecular spin and increase the relaxivity of protons (Fig. 1). **12**@BSA shows not only good stability and biocompatibility, but also exhibits a good T_1 MRI enhancement effect. In addition, **12**@BSA can be used as a photothermal agent for effective tumor elimination.[72]

Pierre's group presented an eight-coordinated stable Fe(II) complex (**13**, Fig. 1) as a dual CA of ^{19}F and chemical exchange saturation transfer (CEST) for ratiometric pH imaging. The intensity of the CEST response depends on the concentration of **13** and pH values, with a significant increase in saturation transfer at pH = 6.9–7.4, while the ^{19}F imaging signal is not pH-dependent. And the rare 8-coordinate geometry Fe(II) complex is stable in air, making the ratiometric pH-mapping and accurate differentiation at pH = 6.9–7.4 being achieved.[73]

3.1.2 Iron complexes as stimuli-responsive MRI agents. The stimuli-responsive agents can selectively detect the analytes and restore their optical or magnetic properties, which makes the imaging of the targets more accurate. These agents have been widely studied recently and are expected to have a bright future. Various stimuli-responsive MRI studies on bioactive species based on iron complexes have also been reported (Fig. 1).[48,49,74–79] The small pH changes in living systems may result in serious diseases, which makes it meaningful to develop pH-responsive probes detecting pH changes at physiological ranges. Gale's group developed a pH-responsive Fe(III)-based MR imaging probe (**14**, Fig. 1) which undergoes relaxivity change *via* pH-mediated control of monomer and dimer morphology. **14** was designed to form a hydroxide coligand at pH $\leq$ 7.4 and self-associate with K_a suitable for *in vivo* MRI, and can interconvert rapidly from a low-relaxivity antiferromagnetically coupled dimeric complex to the high-relaxivity monomeric $S = 5/2$ Fe(III) complex in response to pH changes relevant to human pathophysiology (6.0–7.4). The switches are reversible in response to pH and concentration changes.[74] Some probes are reported to achieve different MRI signals through the valence changes under different redox conditions, which have great potential for resulting in obviously different magnetic properties and leading to large changes in contrast. The same group reported the first example of MRI to pathological changes *in vivo* using redox properties of metal ions. The authors synthesized a redox-active Fe complex (**15**, Fig. 1) as a biochemically responsive MRI CA, which is able to detect tissue inflammation *in vivo*. Hydrogen peroxide (H_2O_2) can rapidly oxidize **15** from Fe(II) to Fe(III), while the conversion between Fe(III) and Fe(II) produces a complete order of magnitude relaxivity change. **15** could rapidly toggle between the Fe(II) and Fe(III) oxidation states in response to L-Cys and H_2O_2, respectively. Injection of **15**-Fe(II) can produce strong and selective tissue contrast enhancement of pancreatitis in a mouse model (caerulein/LPS model), while no significant signal enhancement was observed in normal pancreatic tissue (saline treated mice).[48] Harris's group designed a molecular diiron complex (**16**, Fig. 1), which can achieve quantitation of redox status based on MR. The signals can be achieved through redox-dependent paramagnetic chemical exchange saturation transfer (PARACEST). The diiron **16** under different valence states (+2/+3) is air-stable in aqueous buffer solution, which suggests the possibility for *in vivo* studies.[49]

Besides, switchable spin-crossover Fe complexes have significant potential to be used as OFF/ON mode MRI agents. Some examples using the spin-switching Fe complexes as stimuli-responsive MRI CAs have been reported. Herges's group developed a series of switchable spin-crossover iron complexes. For example, they designed an Fe(III) porphyrin (**17**, Fig. 1) as light-controlled switching MRI with a photochromic axial ligand. The spin state of **17** can be changed reversibly between low-spin ($S = 1/2$) and high-spin ($S = 5/2$) under irradiation of two wavelengths (365 and 435 nm), with the switching efficiency reaching up to 76% at room temperature and no fatigue observed after over 1000 switching cycles. This complex can not only be a simple artificial mimic for the first step of the cytochrome P450 catalytic cycle, but also can be used as an MRI agent with the relaxation time T_1 of water protons switching 15 times as the spin switch. This was the first example of a light-controlled molecular spin switch using an Fe(III) complex.[75] The same group constructed a novel two-component system based on Fe(III) porphyrins bridged with 1,2,3-triazole ligands and one separate ligand (**18**, Fig. 1) for spin switching. The mechanism illustrated that spin state changes happened when the axial ligands changed. During deprotonation, the triazolate anion as the axial ligand coordinating to the Fe(III) makes the complex a high-spin neutral complex, while pyridine coordinating to the second axial coordination site makes **18** change from high-spin to low-spin. Besides, the spin state of the complex can be changed reversibly in the presence of a photoswitchable ligand. **18** can be a potential photoswitchable responsive CA.[76]

Hasserodt's group also published some interesting studies using the spin switchable iron complexes.[77] They designed two binary Fe(II) complexes (**19**–**20**, Fig. 1) of a large ring hexadentate N6 ligand with two picolyl pendent arms with high stability and low-spin diamagnetic state. The probes can detect chemically transforming analytes through reacting with the respective stimulus, the reacted third pendent arm of the complexes will disappear entirely and the new complex will be converted to a high-spin paramagnetic state (from 0 to 2). Therefore, **19** and **20** can successfully detect the analyte and accomplish the spin state changes under simulated physiological conditions.[78] They also prepared a neutral Fe(II) complex (**21**, Fig. 1) with a novel macrocyclic chelator as a CA for MRI, which is the first example of using an iron(II) complex to examine the enhanced MRI contrast *in vitro* and *in vivo* of mice. The results constitute an important step to discover an iron(II)-based CA that passes from the low-spin ($S = 0$, off) to the high-spin ($S = 2$, on) state, upon the presence of and transformation by a specific target enzyme in live animals.[79]

3.1.3 Iron complexes as OI agents. Benefiting from the favorable photophysical properties, iron complexes can also be used for other imaging method-based probes, such as optical and photoacoustic images. Mayilmurugan's group demonstrated a rhodamine appended Fe(III)-catecholate complex **22**

(Fig. 1) as an intelligent dual-modal T_1 MRI-optical imaging probe. The high-spin Fe(III) coordination sphere and rhodamine unit serve as MRI and optical reporters, respectively. **22** was proved to be a potential dual MRI-ON and fluorescence-ON molecular imaging probe to visualize NO and acidic pH in a tumor microenvironment.[80] Two Fe(III) macrocyclic complexes (**23** and **24**, Fig. 1) using 1,4,7-triazacyclononane derivatives as the ligands have been reported by Morrow's group, which could be T_1 relaxation MRI probes. The redox potentials of **23** and **24** are more negative than −200 mV *versus* NHE at neutral pH, which signifies a stable Fe(III) center in a biological environment. The Fe(III) complexes contain a fluorescent label that allows better visualization of uptake and localization in the yeast cells. The fluorescence microscopy and MRI T_1 relaxation studies provided evidence that Fe(III) complexes could be taken into *Saccharomyces cerevisiae* upon electroporation.[67] Tian's group constructed three Fe(II) complexes with triple-pyridyl ligands having different water solubility (**25–27**, Fig. 1). The three complexes are suitable as photoacoustic (PA) probes due to a higher photothermal conversion efficiency resulting from their rapid excited-state deactivation. Notably, **25** possesses high photothermal conversion efficiency reaching up to 29.6%, and excellent PA outcome both *in vivo* and *in vitro*. Further pharmacokinetics evaluation demonstrated that **25** induced minimal invasiveness to living animals, indicating that **25** is suitable for PA imaging *in vivo*.[81]

3.2 Manganese complexes

Manganese is another essential metal ion of life.[82] The water splitting complex of Photosystem II in plants and

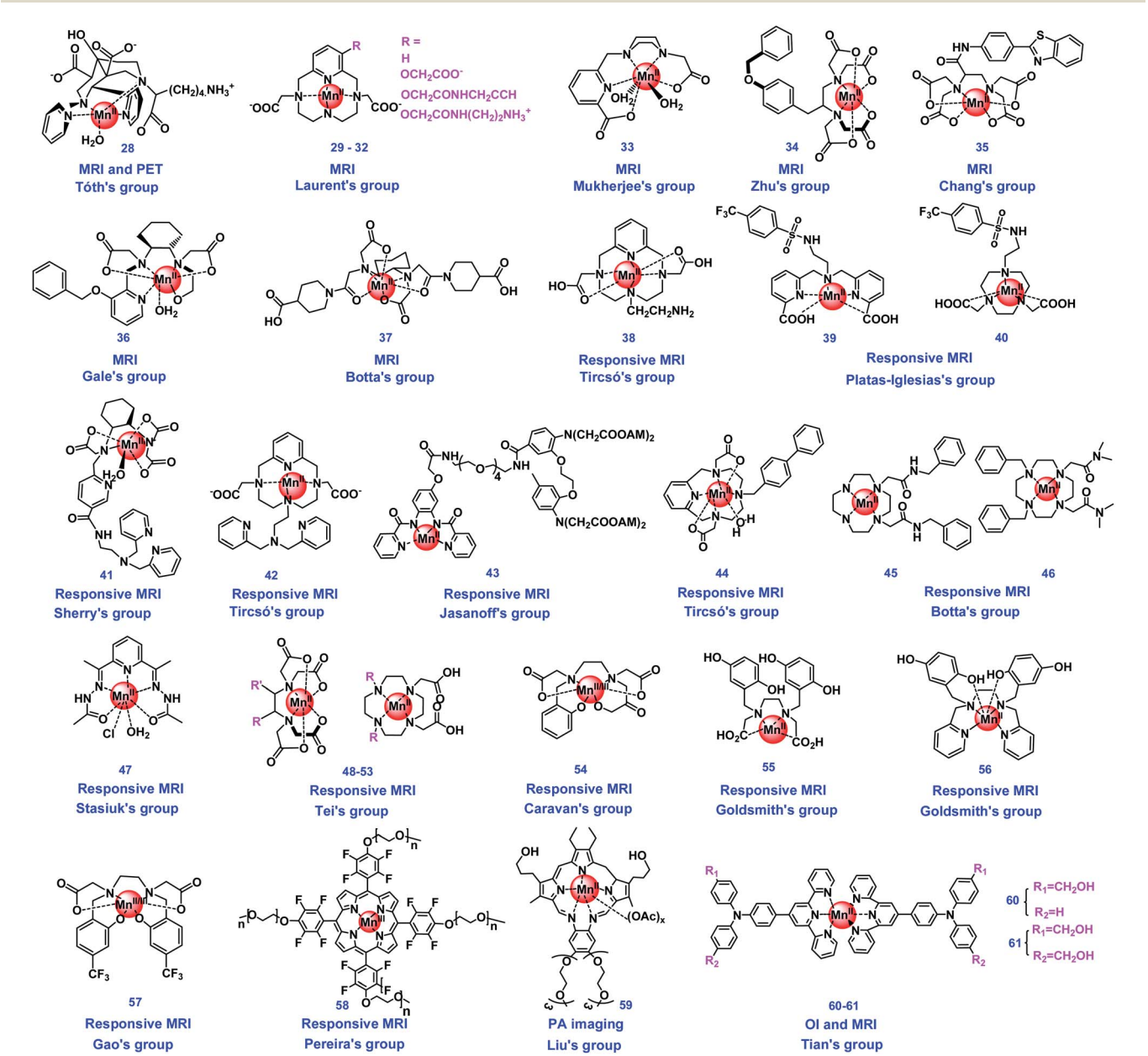

Fig. 2 Chemical structures of manganese complexes used as bioimaging agents.

cyanobacteria, $CaMn_4O_4$, was constituted using manganese as the key element.[83] Besides, manganese is one of the main metals for metalloenzymes,[23] for example, manganese binding superoxide dismutase (Mn-SOD) is one of the main SODs.[32] The oxidation states of manganese are usually +2, +4, and +7.[32] In addition to numerous biomimetic studies utilizing manganese being reported, manganese complex-based bioimaging agents are also constructed in recent years. The structures of Mn complex-based probes summarized in this review are shown in Fig. 2. The properties of these manganese complex-based bioimaging agents have been summarized in Table 2.

3.2.1 Manganese complexes as regular MRI agents. Owing to the various oxidation states of manganese, many reported imaging agents using manganese complexes are MRI probes, and some Mn complexes have already been approved as clinical MRI CAs (*e.g.*, MnDPDP). However, it is still challenging to design new Mn complex-based MRI CAs with high thermodynamic stability. Tóth's group designed and synthesized a Mn(II) complex (**28**, Fig. 2) for MRI with exceptional kinetic inertness. **28** could be stable and did not show any dissociation for 140 days under the condition of 50 eq. Zn^{2+} at 37 °C, pH = 6. The kinetic inertness was considered to be due to the 2,4-pyridyl-disubstituted bispidol ligand coordinated in a five-dentate manner, leaving one coordination site for hydration water, which is important for MRI application, while the non-coordinating pending carboxylates might additionally create a second sphere contribution and increase proton relaxivity. The *in vivo* MRI experiments in mice of **28** were studied, and the Mn content in tissues showed rapid renal clearance. Thus, **28** is a very promising Mn-based imaging agent for MRI and for PET.[84] Laurent's group developed a series of Mn(II) complexes (**29–32**, Fig. 2) binding four 12-membered pyridine-containing macrocyclic ligands based on the pyclen core as CAs for MRI. The properties of these complexes were studied, and the MRI efficacy was also evaluated. The mechanism was studied using ^{17}O NMR and the nuclear magnetic relaxation dispersion profiles, indicating that the four hexadentate ligands prepared left one vacant coordination site to accommodate one water molecule to rapidly exchange to achieve proton relaxivity. The results indicated that the complexes exhibit r_1 relaxivities large enough to be used as clinical MRI CAs.[85] Mukherjee's group demonstrated a pentadentate and bis(aquated) Mn(II) complex (**33**, Fig. 2) as an MRI CA alternative to Gd(III) through inner-sphere water interaction. **33** possesses higher thermodynamic stability compared with previous analogous Mn(II) complexes. DFT calculation indicated that **33** has pentagonal bipyramidal geometry with two water molecules at the axial positions, and the equatorial plane was constituted by the ligand ON_3O donor set. **33** was considered as the possible candidate of a CA through cell viability measurements and phantom MR images using clinical MRI imaging.[86]

To improve the detection contrast, some organ-specific CAs have been developed. Zhu's group constructed a novel Mn(II) complex (**34**, Fig. 2) binding with a lipophilic group-modified ethylenediaminetetraacetic acid (EDTA), as a new liver-specific MRI CA. *In vivo* in mice biodistribution confirmed that **34** can be hepatic specifically ingested with a combination of hepatobiliary and renal clearance pathways. Bromosulfophthalein (BSP) inhibition imaging, biodistribution, and cellular uptake studies confirmed that the amphiphilic anion of **34** promotes the hepatic targeting mediated by organic anion transporting polypeptides (OATPs) expressed by functional hepatocytes. The new CA **34** may contribute to the MRI diagnosis of cancer with altered OATP expression.[87] Chang's group designed and synthesized a novel manganese(II) complex (**35**, Fig. 2) based on an EDTA coordination cage bearing a benzothiazole aniline (BTA) moiety, which was used as a potential liver-specific MRI CA. The liver-specificity was demonstrated because the new Mn chelate could be rapidly taken up by liver hepatocytes and excreted by the kidneys and biliary system. **35** showed much higher kinetic inertness and R_1 relaxivity than MnDPDP, a clinically approved liver-specific MRI CA.[88] Gale's group developed a series of manganese-based CAs containing the ligands of PyC3A derivatives, which were used as liver-specific MRI CAs, and the structure–activity relationships were also studied. Among these complexes, the PyC3A-3-OBn ligand containing **36** (Fig. 2) emerged as the lead candidate due to the properties of high relaxivity, rapid blood clearance, and avid hepatocellular uptake. **36** can render liver tumors conspicuously hypo-intense in a murine model and be wholly eliminated within 24 h of injection. The SAR generated in this study suggested that liver specific properties could be affected by the log *P* values.[89]

Owing to the development of nanotechnology, many medical studies used nanoparticles as carriers. As for the MRI agents, some complexes were loaded onto nanomaterials to increase the relaxivity of complexes. Botta's group obtained novel Mn(II)-based nanoprobes as high contrast enhancing agents MRI by anchoring a Mn(II)-CDTA derivative (**37**, Fig. 2) to the surface of organo-modified silica nanoparticles (SiNPs). High image contrast was found for the **37**-based nanoprobes in T_{1w}-MRI images collected on phantoms containing relatively small amounts of CA, and low cellular toxicity was observed. Preliminary *in vivo* studies demonstrated the efficiency of the **37**-based nanoparticle as T_{1w}-MRI probes, resulting in significant contrast enhancement in the liver.[90]

3.2.2 Manganese complexes as stimuli-responsive MRI agents. In addition to the regular MRI CAs, the development of intelligent CA candidates for MRI has become the new trend, and the studies using responsive bioimaging agents are active in recent research, especially those with changeable oxidation states. Some pH-sensitive manganese complex-based MRI agents have been studied. Tircsó's group constructed the first Mn(II) complex-based MRI agent that can be activated by changing the pH of its local environment. The Mn(II) complex (**38**, Fig. 2) was synthesized using an ethylamine pendant arm as ligand, and was highly thermodynamically stable and kinetically inert. **38** showed a relatively slow water exchange rate, while the pH-dependent coordination of the ethylamine moiety on **38** occurs at pH 6–8, enabling the complex to exhibit pH-sensitive relaxivity in the biologically relevant pH range, because of the appearance of the metal-bound water molecule. The favorable kinetic and relaxometric properties of **38** make it useful as a pH-sensitive MRI CA.[91] Platas-Iglesias's group

Table 2 Manganese complexes as bioimaging agents

Imaging agents	Type of agent	Contrast/fluorescence enhancement	Magnetic field	Relaxivity (mM^{-1} s^{-1})	Detection mechanisms	Targets	Ref
28	MRI and PET	$\Delta r_1 = 1.75$ mM^{-1} s^{-1} increased in human serum	4.7 T, 37 °C	$r_1 = 3.37$	Proton relaxation of inner- and second-sphere water interacted with Mn	*In vivo* imaging	84
29–32	MRI	—	9.4 T, 37 °C	r_1 = **29**: 2.8; **30**: 2.7; **31**: 3.1; **32**: 2.95	Proton relaxation of inner sphere water interacted with Mn	Potential to be clinical MRI CAs	85
33		Increase with the increase of concentration	1.41 T, 25 °C	$r_1 = 4.28$			86
34		$\Delta r_1 = 11.47$ mM^{-1} s^{-1}	0.47 T, 32 °C	**34**: $r_1 = 4.34$, **34**/BSA: $r_1 = 15.81$	Proton relaxation; binding with BSA	Liver specific imaging	87
35		$\Delta r_1 = 11.6$ mM^{-1} s^{-1}	1.5 T, 24 °C	**35**: $r_1 = 3.5$, **35**/HSA: $r_1 = 15.1$		Liver targeting, tumor imaging	88
36		$\Delta r_1 = 6.6$ mM^{-1} s^{-1}	1.4 T, 37 °C	In Tris: $r_1 = 2.4$, in plasma: $r_1 = 9.0$	Proton relaxation	Liver tumor	89
37	MRI	$\Delta r_1 = 15.0$ mM^{-1} s^{-1}	0.5 T, 25 °C	**37**: $r_1 = 3.5$, **37**/SiNPs: $r_1 = 18.5$	Proton relaxation, inner sphere water interaction with Mn(II)	Low field (up to 1.5 T) MRI applications *in vitro* and *in vivo*	90
38	pH responsive MRI	$\Delta r_1 = 1.4$ mM^{-1} s^{-1}	0.49 T, 25 °C	pH 8.4: $r_1 = 2.1$, pH 6.0: $r_1 = 3.5$		pH *in vitro*	91
39, **40**		$\Delta r_1 = 6.0$ mM^{-1} s^{-1}	0.5 T, 25 °C	pH 9.0: $r_1 = 3.8$, pH 4.0: $r_1 = 9.8$		pH *in vitro*	92
41	Metal-sensitive MRI	$\Delta r_1 = 13.7$ mM^{-1} s^{-1}	1.4 T, 37 °C	**41**: $r_1 = 3.7$, **41** + Zn^{2+} + HSA: $r_1 = 17.4$	Proton relaxation; binding with Zn^{2+} and BSA	Glucose-stimulated zinc secretion from the mouse pancreas and prostate	93
42		$\Delta r_1 = 5.92$ mM^{-1} s^{-1}	1.41 T, 37 °C	**42**: $r_1 = 3.11$, **42** + Zn^{2+} + HSA: $r_1 = 9.03$		Glucose-stimulated zinc	31
43		$\Delta r_1 = 1.5$ mM^{-1} s^{-1}	—	**43**: $r_1 = 3.6$, **43** + Ca^{2+}: $r_1 = 5.1$	Proton relaxation; binding with Ca^{2+}	Intracellular Ca^{2+} sensing	94
44	HSA-sensitive MRI	$\Delta r_1 = 31.9$ mM^{-1} s^{-1}	0.49 T, 37 °C	**44**: $r_1 = 3.8$, **44** + HSA: $r_1 = 35.7$	Proton relaxation; inner sphere water interaction with Mn(II) and HSA	HSA of vascular	95
45, **46**		$\Delta r_1 = 15.7$ and 24.6 mM^{-1} s^{-1} for **51** and **52**, respectively	0.5 T, 37 °C	$r_1 = 2.8$ for both $r_1 = 18.5$, 27.4 with HSA		HSA	96
47	BSA-sensitive MRI	$\Delta r_1 = 15.4$ mM^{-1} s^{-1}	0.5 T, 25 °C	$r_1 = 5.7$, $r_1 = 21.1$ with HSA		BSA	97
48–53	MRI	Increased 1.8–13.3 fold	0.75 T, 25 °C	r_1 values for **48–53**: 4.6, 5.9, 18.4, 2.2, 12.6, 15.3		HSA binding enhanced MRI	98
54	Redox-active MRI	3-fold increase in relaxivity	4.7 T, 37 °C	—	Exchange between Mn(II) and Mn(III)	GSH and H_2O_2	99
55		—	—	—	Proton relaxation; inner sphere water interactions	H_2O_2	100
56		$\Delta r_1 = 1.71$ mM^{-1} s^{-1}	3 T, 25 °C	$r_1 = 5.46$, $r_1 = 7.17$ with H_2O_2		H_2O_2	101

Table 2 (*Contd.*)

Imaging agents	Type of agent	Contrast/fluorescence enhancement	Magnetic field	Relaxivity (mM^{-1} s^{-1})	Detection mechanisms	Targets	Ref
57		$\Delta r_1 = 2.0$ mM^{-1} s^{-1}	0.5 T, 37 °C	Mn(II): $r_1 = 0.7$, Mn(III): $r_1 = 2.7$	$^1H/^{19}F$ MRI	GSH and H_2O_2	102
58		Obviously enhanced for Mn(II)	0.5 T, 25 °C	Mn(II): $r_1 = 24.3$	Exchange between Mn(II) and Mn(III)	Ascorbic acid or β-mercaptoethanol, O_2	103
59	PA	Intensity increased 3.1-fold 24 h after injection	—	—	Nonradiative conversion of light energy	RAW 264.7 cells and *in vivo*	104
60, 61	OI and MRI	—	—	—	Two-photon OI and MRI	*In cellulo* and *ex vivo*	105

presented two sulfonamide groups containing Mn(II) complexes (**39** and **40**, Fig. 2) which were conceived as potential pH-responsive MRI agents. The electron-withdrawing CF_3 group of ligands pushed the pK_a of the sulfonamide group to the biologically relevant range. **39** and **40** showed different thermodynamic stabilities and relaxometric behaviors. **40** dissociated at a relatively high pH, while the relaxivity of **39** increased because of the protonation of the sulfonamide group in the physiologically relevant pH window, and relaxivity increased due to protonation related to coordination of a second H_2O. This proton binding process of sulfonamide group is reversible.[92]

Some metal ion-sensitive MRI studies have also been reported. Sherry's group prepared a Mn(II)-based zinc-sensitive MRI CA (**41**, Fig. 2) to detect glucose-stimulated zinc secretion (GSZS) from the mouse pancreas and prostate *in vivo*. **41** was revealed to have superior kinetic inertness from the thermodynamic and kinetic stability experiments, compared with GdDTPA. When compared with other gadolinium-based zinc sensors, **41** appeared to be an alternative for β-cell function images in the pancreas, and GSZS from the prostate. The two BPEN moieties each bound with a single Zn^{2+} ion resulted in a new complex forming a ternary complex with albumin, which resulted in an increase of r_1 relaxivity.[93] Tircsó's group presented another zinc-responsive Mn(II)-based MRI CA candidate (**42**, Fig. 2) derived from pyclen-3,9-diacetate (3,9-PC2A) possessing a di(2-picolyl)amine (DPA) moiety as an active arm. **42** has a relatively high relaxation rate, which cannot be affected by the zinc concentration directly, however, in the co-presence of 0.7 mM human serum albumin (HSA), the relaxation rate values increased significantly owing to the efficient binding of **42** to the protein. The increase can be visualized by MRI experiments *in vitro*, and *in vivo* tests confirmed that GSZS could be observed in the prostate of a healthy mouse.[31] Jasanoff's group developed a Mn-based MRI CA (**43**, Fig. 2) as a sensor for intracellular calcium ions (Ca^{2+}). This cell-permeable complex will undergo esterase cleavage, and allow intracellular Ca^{2+} levels to be monitored by MRI. Their results indicated that **43** is a Ca^{2+} sensor that can achieve spatiotemporal mapping of calcium signaling processes, and possess the properties of being compatible with the extensive expanded depth and field of view afforded by MRI.[94]

Some studies reported enhanced relaxivity while the complexes bind with proteins. Tircsó's group prepared a macrocyclic chelate Mn(II) complex (**44**, Fig. 2) which possesses high thermodynamic stability and kinetic inertness as well as remarkable relaxivity in the presence of HSA. These properties make **44** have a significant MRI signal intensity increase in the vasculature even at low dose of it.[95] Botta's group synthesized two novel macrocyclic ligands Mn(II) based on the 1,4-DO2AM platform and containing two benzyl groups (**45** and **46**, Fig. 2), which could form relatively strong adducts with HSA. The interaction with HSA slows down the rotational tumbling of **45** and **46** in solution, resulting in adducts endowed with remarkably high proton relaxivities.[96] Stasiuk's group developed a Mn(II)-based T_1 CA (**47**, Fig. 2) with a Schiff-base type diacetylpyridylcarbo-hydrazide ligand using a simple single-pot

template reaction. **47** displays optimized r_1 relaxivities at both medium (20 and 64 MHz) and high (300 and 400 MHz) magnetic fields. Upon binding to BSA ($K_a = 4.2 \times 10^3$ M^{-1}), a much enhanced r_1 value was achieved. The studies *in vivo* showed that **47** could be cleared intact into the bladder through renal excretion, and has a prolonged blood half-life compared to commercially avaliable Gd CA Magnevist.[97] Tei's group reported that the Mn(II) complexes of six original amphiphilic ligands (three EDTA-like ligands and three 1,4-DO2A derivatives) embodying one or two aliphatic chains (**48–53**, Fig. 2) were evaluated as potential MRI CAs. The relaxivity (r_1) enhancement was observed for the Mn(II) micelles, resulting from the increased molecular tumbling rate of the supramolecular aggregate. **48–53** could bind to HSA tightly using their amphiphilic chelates with large association constants, and achieved remarkable relaxivity values.[98]

Some studies reported the detection of bioactive species using Mn complexes, with the relaxivity changing along with the change of the Mn oxidation state. Caravan's group has reported a simple Mn coordination complex (**54**, Fig. 2) as a redox-activated MR CA in 2013; the Mn(II)/Mn(III) redox couple could convert reversibly in the presence of glutathione (GSH) and H_2O_2 followed by relaxivity changes.[99] Goldsmith's group designed a Mn(II) complex (**55**, Fig. 2) with quinol-containing ligands as MRI CA sensors to H_2O_2. The metal center could be oxidized by H_2O_2 to the less paramagnetic Mn(III), which can eliminate the r_1 response of this complex.[100] Upon modifying the ligand, H_2O_2 may oxidize the ligand and result in the opposite relaxivity changes. The same group reported another redox-responsive mononuclear Mn(II) complex (**56**, Fig. 2) as a MRI CA by using the ligand with two quinols. The introduction of the second quinol improves the relaxivity response of **56** to H_2O_2 and reduces its cytotoxicity. The authors found that H_2O_2 can partially oxidize the quinol subunits to *para*-quinones, and the oxidation of the ligand enables more H_2O to coordinate with the metal ion due to *para*-quinones being unable to deprotonate to an anionic form, resulting in the enhancement of relaxivity.[101]

Gao's group prepared a redox-responsive manganese complex (**57**, Fig. 2), which can convert the Mn(III)/Mn(II) couple reversibly by GSH and H_2O_2, respectively. The complexes in both states are water soluble and biologically interconvertible. Therefore, **57** can be used as a probe in $^1H/^{19}F$ MRI for detecting and imaging biological redox species. Mn(III)/Mn(II) in this system have been demonstrated to be a redox reversible couple. This work provides a pathway to access redox information associated with various diseases.[102] Pereira's group constructed a biocompatible redox MRI probe based on a Mn porphyrin complex (**58**, Fig. 2). The complex can reversibly switch between Mn(II)/Mn(III) oxidation states in aqueous solutions. The Mn(III) ion can be reduced to the Mn(II) form in the presence of ascorbic acid or β-mercaptoethanol, and the Mn(II) would be slowly but fully reversed back to Mn(III) in the presence of O_2. This redox imaging probe showed good water solubility, biocompatibility, non-toxicity, and a strong "turn on" relaxivity response upon reduction.[103]

3.2.3 Manganese complexes as OI agents. Moreover, Mn complexes can be also used as optical and PA imaging agents considering their good photophysical properties. For example, Liu's group explored the NIR absorptivity of the metallotexaphyrin complexes for PA-based imaging. Among the three complexes binding with manganese(II), gadolinium(III), and lutetium(III), the Mn-binding complex (**59**, Fig. 2) provided the greatest PA signal intensities in both water and RAW 264.7 cells. The enhanced PA-based imaging for **59** was demonstrated by the experiments *in vivo* of a prostate mouse model tumor and provided complete 3D diagnostic information. **59** showed excellent *in vivo* stability allowed for PA-based imaging of tumors with no adverse toxicity to major organs. Based on the results above, **59** may be an effective probe either as a stand-alone PA/CA or as a single molecule dual-modal (PA and MR) imaging agent for tumor diagnosis.[104] Tian's group constructed two Mn(II) compounds (**60** and **61**, Fig. 2) for combined fluorescence and MR imaging. Both of the two complexes showed an enhanced stable two-photon signal and magnetic contrast. **60** demonstrated multi-modal imaging effectiveness based on its d^5 electron configuration, and the complex possesses the capability of not only good penetration into thick tissue with an enhanced magnetic signal, but also two-photon imaging and stimulated emission depletion (STED) super-resolution imaging. This is the first demonstration of fluorescence and MR cross-platform imaging in cells and solution using a Mn complex.[105]

3.3 Copper complexes

Copper is the third most abundant essential trace metal for life, which usually exists through binding with proteins to form metalloproteins.[20] Similar to the two metal ions discussed above, copper complexes can be the catalytic center of some metalloenzymes, such as copper, zinc-superoxide dismutase (Cu, Zn-SOD).[106] Copper also plays a vital role in other living possesses, including gene expression, electron transfer and redox processes, to maintain the metabolism of life.[107] The imaging studies using copper complexes have attracted much attention in recent decades through both optical and MR imaging. The structures of Cu complex-based probes summarized in this review are shown in Fig. 3, and their properties have been summarized in Table 3.

3.3.1 Copper complexes as regular OI agents. Copper complex-based probes are commonly reported as OI agents. Manivannan's group designed a Cu(II) sensor using 3-(2-hydroxyphenyl) imidazo[5,1-*a*]isoquinoline (LH), which in turn can selectively detect the cyanide ion (CN^-). An obvious color change could be observed from colorless to yellowish green with LH bound with Cu(II). As a result, the $[Cu(L)_2]$ complex (**62**, Fig. 3) can detect CN^- over other anions through removal of copper and formation of the insoluble $[CuCN]_x$, along with the obvious color changes. The cellular images using MDA-MB-231 showed that intracellular Cu(II) and CN^- can be detected using LH and **62**, respectively.[108] Shang's group demonstrated four Cu(II) complex-based colorimetric fluorescent probes (**63–66**, Fig. 3) with the crystal structures characterized using X-ray diffraction. The synthesized probes showed significant colour changes and remarkable increase of fluorescence intensity (over

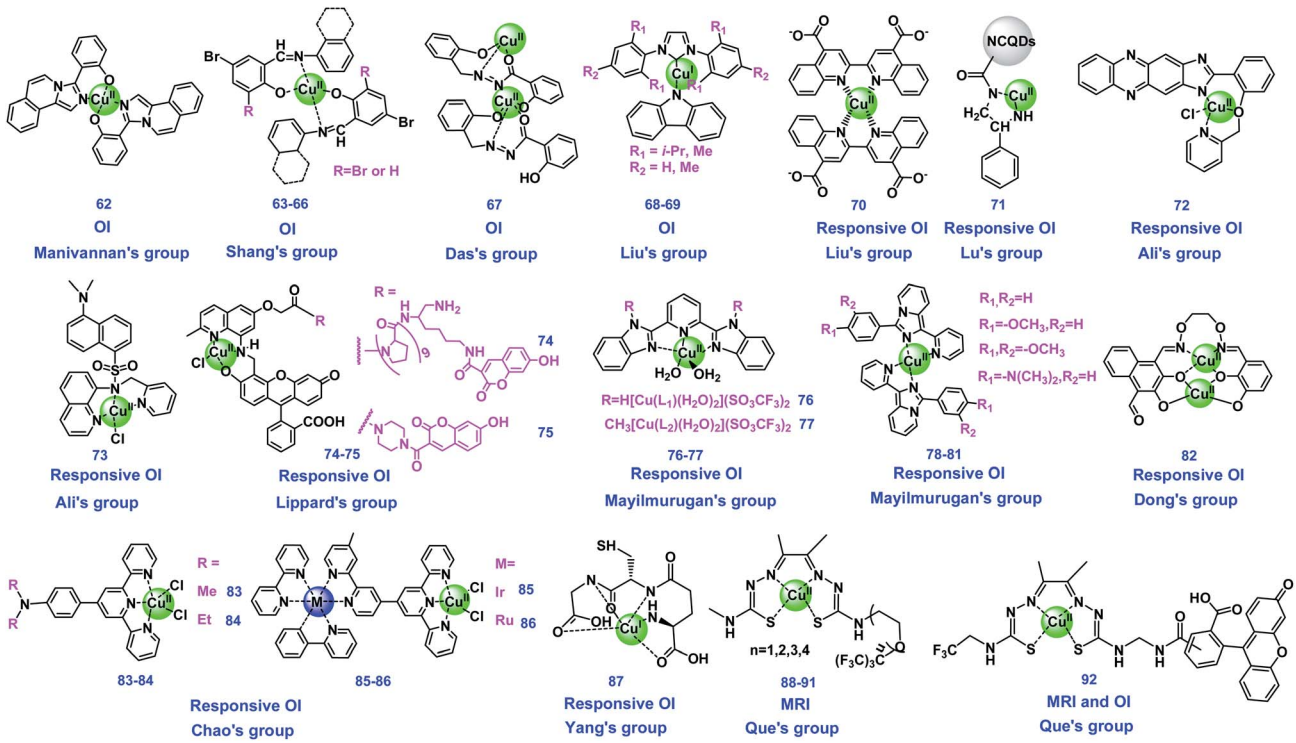

Fig. 3 Chemical structures of copper complexes used as bioimaging agents.

80-fold) in the presence of HS^-. During the detection process, HS^- captured the copper ion and the free ligand was released, followed by the increased fluorescence. Cytotoxicity studies in HeLa cells indicated that **63–66** have low cytotoxicity and have the potential to be used to detect H_2S levels *in vivo*.[109] Das's group prepared a polynuclear Cu(II) complex (**67**, Fig. 3) and used for real time monitoring of cytochrome C (Cyt C) release from mitochondria during cellular apoptosis. **67** was synthesized using a new amide–imine conjugate, 2-hydroxybenzoic acid-(2-hydroxybenzylidene)-hydrazide, and characterized using single crystal X-rays. Since the non-fluorescent **67** has high affinity with Cyt C, the selective and spatial interaction of **67** and Cyt C results in the turn-on fluorescence. Then the fluorescence imaging of intracellular events in living cells was realized using **67**. Finally, for the first time, the direct visualization of Cyt C translocation during apoptotic processes was achieved.[110] Liu's group reported two novel two-coordinated Cu(I)–N-heterocyclic carbene (NHC) complexes (**68–69**, Fig. 3). The complexes exhibited unique fluorescence and phosphorescence dual-emission properties. The structures and mechanisms have been studied and compared. The emissive mechanism was proved to be the singlet/triplet locally excited state of the carbazole group, which is different from the general luminescence mechanisms (MLCT, XLCT or ICT). This study proved that the two-coordinate Cu(I)–NHC complexes can be used as potential candidates for ultralong room-temperature phosphorescence (RTP).[111]

3.3.2 Copper complexes as stimuli-responsive OI agents. Many studies detect the targets through reacting the copper complexes with the bioactive molecules and changing the valence of copper ions. Such stimuli-responsive imaging agents could reduce Cu(II) ions to Cu(I), and restore the fluorescence through the pathways such as: changing the photophysical properties of the complexes, demetallization to generate photosensitizers from the ligands, and aggregation of the reduced complexes. This part is the main developing strategy for recent Cu-based OI probes.

The photophysical properties and fluorescence mechanisms of copper complexes may change as the metal valence changed. Liu's group developed a colorimetric alkaline phosphatase (ALP)-linked immunoassay method for highly sensitive determination of rabbit IgG and prostate specific antigen (PSA) using a Cu(II)-BCA (**70**, Fig. 3) based color generation system. In the presence of IgG or PSA, ALP was introduced to catalyze L-ascorbic acid 2-phosphate (AAO) to L-ascorbic acid (AA), which results in Cu(II) of **70** being reduced to Cu(I). The reduced Cu(I) species of **70** showed a purple color, and was utilized as a promising chromogenic reporter for the visual immunoassay. This method holds many advantages, and provides a promising colorimetric immunoassay platform for bio-chemical analysis in different fields.[112] Lu's group constructed a Cu(II)-functionalized nanoplatform by coupling a Cu(II) complex with L-phenylalaninamide (LPN) (**71**, Fig. 3) with N-doped carbon quantum dots (LPQDs), which was used as mimetic-peroxidase with catalytic properties for sensitive monitoring of H_2O_2. The detection of H_2O_2 in biological samples could be realized with the detection limits of 80 nM and 2.5 μM by colorimetric and fluorescent methods, respectively, through capturing the appearance of colorimetric and fluorescence changes. During the H_2O_2 detection process, Cu(I)-LPQDs may form through

Table 3 Copper complexes as bioimaging agents

Imaging agents	Type of agents	Contrast/fluorescence enhancement	Magnetic field	Relaxivity (mM^{-1} s^{-1})	Detection mechanisms	Targets	Ref
62	OI	Obvious color change	—	—	Colorless to yellowish green	CN^-	108
63–66		Over 80-fold increase of fluorescence intensity	—	—	Color change and fluorescence enhancement	HS^-; H_2S level *in vivo*	109
67		156-fold fluorescence enhancement after incubation with Cyt C	—	—	Interaction with Cyt C, fluorescence enhancement	Cytochrome C (Cyt C)	110
68–69		RTP is achieved with a lifetime of 140 ms	—	—	Fluorescence and phosphorescence dual-emission	—	111
70	Stimuli-responsive OI	The LODs of rabbit lgG and PSA are 0.05 ng mL^{-1} and 0.38 ng mL^{-1}, respectively	—	—	Reduction of Cu(II) to Cu(I), colorimetric and fluorescence methods	Rabbit IgG and prostate specific antigen (PSA)	112
71		The LODs of H_2O_2 by colorimetric and fluorescent methods are 80 nM and 2.5 μM	—	—	Cu(I) may be formed Cu(II)-LPQDs; colorimetric and fluorescence changes	H_2O_2	113
72		5-fold and 6-fold fluorescence enhancement upon treatment with NO and HNO, respectively	—	—	Reduction of Cu(II) to Cu(I) resulted in a remarkable fluorescence recovery	NO and HNO	46
73		Fluorescence intensity restored up to six-fold (90%)	—	—	Fluorescence enhancement through PET	HNO	114
74, 75		11-fold ratiometric turn-on	—	—	Cu(II) reduced to Cu(I), de-metallization, and N-nitrosated ligand products recovered fluorescence	Ratiometric detection of NO	115
76, 77		The fluorescence intensity of **76** and **77** increased 28 and 143 times, respectively	—	—	Reduction of Cu(II) to Cu(I) and the displacement of copper recovered fluorescence	Cys	116
78–81		The fluorescence intensity increased 103-fold in the presence of Cys	—	—	Reduction of Cu(II) to Cu(I) resulted in fluorescence recovery	Cys	117
82		The LODs of $S_2O_3^{2-}$ and GSH are 149 and 131 nM, respectively	—	—	Cu(II) was reduced to Cu(I), released free ligand, and fluorescence recovered by the ICT process	$S_2O_3^{2-}$ and GSH	118
83–86		1500-fold luminescence intensity enhancement of **84** in the detection of Hcy	—	—	Cu(II) was reduced by Hcy to form four-coordinated terpyridine-Cu(I) and recovered luminescence	Hcy	119
87	OI (and PET)	—	—	—	Luminescent Cu(I) oxidized to non-luminescent Cu(II)	Oxidation states *in vivo*	120
88–91	^{19}F MRI	T_2-increase of 129-fold between one of the Cu^{2+} complexes and its reduced system	7.0 T, 22 °C	—	Hypoxia-targeting ^{19}F MRI	Hypoxia cells	124
92	^{19}F MRI and OI	The SNR of ^{19}F increased 7-fold and the fluorescence intensity increased 3.5-fold in hypoxia	—	—	^{19}F MR and fluorescence signals being turned on when reduced to Cu(I)	Hypoxic cells	122

discharging electrons by aromatic species in LPQDs into Cu(II)-LPQDs. These findings provide clues for the construction of intelligent biomimetic nanoplatforms using copper for sensing applications and exhibit high peroxidase mimetic activity.[113] Ali's group synthesized a phenazine-based Cu(II) complex (**72**, Fig. 3) for the selective detection of NO and HNO in biological systems. **72** was nonfluorescent, however, fluorescence can remarkably regenerate upon treatment with NO and HNO under physiological conditions, where **72** was reduced to Cu(I) species. The photophysical properties of the ligand and complexes have been studied using DFT. **72** was found to be almost nontoxic and cell permeable, making it available to image the exogenous and endogenous NO and HNO in A549 and Raw 264.7 cells.[46] The same group also synthesized a novel Cu(II) complex-based fluorescent probe (**73**, Fig. 3) which exhibits a high selectively significant fluorescence turn-on response towards HNO. HNO can induce the reduction of paramagnetic **73** to diamagnetic Cu(I) species with fluorescence obviously enhanced through the photoinduced electron transfer (PET) mechanism. Additionally, **73** could detect HNO effectively in the biological pH range, and the properties of water friendliness, low cytotoxicity and cell permeability, make **73** useful for the detection of HNO in living cells.[114]

The reduction of Cu(II) to Cu(I) can result in displacement of the complexes, and the fluorescence will be restored along with the free ligands, which probably further reacted with the bioactive molecules. Lippard's group presented the first two Cu(II)-based fluorescent sensors (**74** and **75**, Fig. 3) for direct ratiometric detection of nitric oxide (NO), which is one of their series of studies of directly imaging NO production in living cells by turn-on Cu(II)-based fluorescence. The probes work by energy transfer between hydroxycoumarin and fluorescein chromophores by a FRET mechanism, containing polyproline or piperazine as rigid spacers. In the presence of NO, the Cu(II) of probes was reduced to Cu(I), followed by amine deprotonation and nitrosation, and the fluorescence was restored for the N-nitrosated products. Notably, they elicited a rapid and selective ratiometric response upon direct reaction with NO at physiological pH values.[115]

Mayilmurugan's group constructed two Cu(II) complexes (**76** and **77**, Fig. 3) using 2,6-bis(benzimidazolyl)pyridine derivatives as the ligands, for highly L-cysteine (Cys) selective "turn-on" optical probes. The properties of **76** and **77** were compared, and both of them showed selective and efficient "turn-on" fluorescence behavior in the presence of Cys over other amino acids. The detection was realized by the reduction of the Cu(II) center to Cu(I) followed by the displacement of copper.[116] They also synthesized four imidazopyridine-based Cu(II) complexes (**78–81**, Fig. 3) as turn-on OI probes for Cys in cancer cells. The molecular structures of these complexes were studied using different techniques. The detection studies indicated that **79** showed selective and efficient turn-on fluorescence behavior towards Cys among the probes. The selective detection may originate from a nearly perfect trigonal plane of **79** adopted around a Cu(II) center, which required minimum structural change during the reduction of Cu(II) to Cu(I) when imaging Cys, while other complexes need more reorganizational energy. **79** was used for OI of Cys in HeLa cells and macrophages.[117] Dong's group designed and exploited a novel turn-on fluorogenic aldehyde-appended salamo-like Cu(II) complex (**82**, Fig. 3) for the simultaneous detection of thiosulfate ($S_2O_3^{2-}$) ions and GSH through an intramolecular charge transfer (ICT) process. **82** showed highly selective and sensitive fluorescence recovery towards $S_2O_3^{2-}$ and GSH in aqueous DMF medium with the detection limits of 149 and 131 nM, respectively. During detection of $S_2O_3^{2-}$ and GSH, Cu(II) was reduced to Cu(I) ions and displaced from the coordination sphere, resulting in the release of the free ligand.[118]

Some luminescent Cu(I) complexes as probes have been reported owing to the changeable valence states. Chao's group designed four terpyridine-based Cu(II) complexes (**83–86**, Fig. 3) for the detection of homocysteine (Hcy) in water and cells through aggregation enhanced luminescence. **84** and **86** were found to have better performance than **83** and **85**. The enhanced luminescence was because these Cu(II) complexes were reduced by Hcy to form four-coordinated terpyridine-Cu(I) species, while the aggregation of reduced **83** and **85** enhanced the inhibition of oxygen-induced luminescence quenching. The cellular imaging experiments revealed that **84** could localized in the whole, while **86** only stained cytoplasm.[119] Some redox-active ligands can be oxidized together with the metal ions to generate new complexes. For example, Yang's group demonstrated a luminescent glutathione-mediated Cu(I) complex (Cu(I)-GSH, **87**, Fig. 3) for *in vivo* imaging studies. **87** was revealed to have much more efficient renal clearance and obviously lower liver accumulation than that of its oxidation states, which may be due to the strong protein binding capability of the partial Cu(II)-GSSG complex formed. The radioactive **87** have the potential to be a PET imaging agent in clinical translation.[120]

3.3.3 Copper complexes as MRI or dual-modal agents. Copper complexes can also be used as MRI agents, owing to the electron configuration and valence state changes of Cu, among which ^{19}F MRI is commonly reported. The copper complex-based MRI or dual-modal imaging agents is another developing trend. Que's group carried out a series of experiments using copper complexes for MRI studies.[51,121–123] For example, they presented four fluorinated Cu(II) ATSM derivatives (**88–91**, Fig. 3) for potential use as ^{19}F MR agents for sensing hypoxia in cells. These complexes have a hypoxia-targeting Cu(II) coordination core, and nine equivalent fluorine atoms connected *via* a variable-length polymer linker. The fluorine moiety with a long linker maintains the coordination geometry of Cu(II) complex, which modulates the Cu(II/I) reduction potential, ^{19}F NMR relaxation properties, and lipophilicity. ^{19}F MR phantom imaging and ^{19}F NMR demonstrated the potential utility of these complexes, including in intact live cells.[124] They also constructed a Cu(II)-based ^{19}F MRI and fluorescence imaging dual-responsive probe (**92**, Fig. 3) for detecting cellular hypoxia. This probe had no ^{19}F MR signal and a reduced fluorescence signal due to Cu(II) paramagnetic quenching, while both modes being turned on when reduced to Cu(I). This bimodal agent could be used to differentiate hypoxia cells from the normal ones.[122]

There are also some reports using copper complexes to make biosensors, such as nano copper complexes as a potentiometric membrane biosensor for the early detection of the prostate-specific antigen (PSA).[48] And the studies using the copper complexes as theranostic agents are also reported.[47,125–127]

4. Conclusion and perspectives

In summary, redox-active transition metal complexes have shown great potential as bioimaging agents through optical or MR imaging modalities owing to their diverse structures and functions. We overviewed the development and bioimaging applications of molecular probes based on iron, manganese, and copper complexes in recent five years. Some of these probes have been approved as clinical MRI CAs (*e.g.*, MnDPDP). These probes can be activated in biological systems by different bioactive species, including H_2O_2, H_2S, pH, hypoxia, proteins *etc.*, through the changes of responsive metal ions or ligands. However, the research in this field is still in its infancy, and many unresolved problems and challenges remain to be solved.

We propose that the potential future development of this field could include the following directions: (1) the development of more dual/multi modal bioimaging agents. Each detection modality has its shortcomings, while the agents combining imaging modalities of optical and MR were expected to avoid the shortages and maintain their advantages. Besides, combined with the two imaging technologies, the rationally designed molecular probes could image the subcellular organelles and biomolecules more accurately. Although a few complex-based dual modal probes have been reported, developing more efficient agents with the combination of different advantages is still challenging. (2) Design of "double/multi-locked" bioimaging agents. The "single-locked" imaging agents that only respond to single stimulus may suffer from false positive signals of the normal cells/tissues. The agents that can respond to double even multiple stimuli can efficiently increase the detection accuracy. (3) The imaging application of these bioimaging agents can be extended. The transition metal complexes possess many specific advantages compared with organic molecular probes, therefore many other applications, such as the lifetime imaging, CT, ultrasound imaging *etc.*, could be achieved. And the real-time dynamic imaging and imaging for deeper tissues, which are challengeable for current imaging studies, are expected to be overcome. (4) Finally, it is necessary to investigate the structure–activity relationship (SAR) of metal complex-based bioimaging agents systematically, and further explore the possibility of their clinical translation. Some manganese probes have been proved for clinical usage, however, more transition metal complex-based probes for clinical translation are needed. We believe that more novel efficient probes based on transition metal complexes will be developed for bio-applications in the following years.

Author contributions

B. Tang and N. Li proposed the conception, and led the project; S.-S. Xue and Y. Pan drafted the manuscript; all the authors wrote and revised the manuscript.

Conflicts of interest

There are no conflicts to declare.

Acknowledgements

This work was supported by Shandong Provincial Key Research and Development Program (Major Scientific and Technological Innovation Project) (2021CXGC010515) and Youth Innovation Science and Technology Program of Higher Education Institution of Shandong Province (2019KJC022).

Notes and references

1 W. G. Kaelin Jr and C. B. Thompson, *Nature*, 2010, **465**, 562–564.
2 L. Satriano, M. Lewinska, P. M. Rodrigues, J. M. Banales and J. B. Andersen, *Nat. Rev. Gastroenterol. Hepatol.*, 2019, **16**, 748–766.
3 H. Sies and D. P. Jones, *Nat. Rev. Mol. Cell Biol.*, 2020, **21**, 363–383.
4 J. Muri and M. Kopf, *Nat. Rev. Immunol.*, 2021, **21**, 363–381.
5 C. Gorrini, I. S. Harris and T. W. Mak, *Nat. Rev. Drug Discovery*, 2013, **12**, 931–947.
6 T. C. Jorgenson, W. Zhong and T. D. Oberley, *Cancer Res.*, 2013, **73**, 6118–6123.
7 Y. Yang, Q. Zhao, W. Feng and F. Li, *Chem. Rev.*, 2013, **113**, 192–270.
8 L. Wu, J. Liu, P. Li, B. Tang and T. D. James, *Chem. Soc. Rev.*, 2021, **50**, 702–734.
9 A. Gupta, P. Caravan, W. S. Price, C. Platas-Iglesias and E. M. Gale, *Inorg. Chem.*, 2020, **59**, 6648–6678.
10 L. Wu, F. Liu, S. Liu, X. Xu, Z. Liu and X. Sun, *Int. J. Nanomed.*, 2020, **15**, 7377–7395.
11 G. Katti, S. A. Ara and A. Shireen, *Int. J. Dent. Clin.*, 2011, **3**, 65–70.
12 H. Lusic and M. W. Grinstaff, *Chem. Rev.*, 2013, **113**, 1641–1666.
13 S. D. Rawson, J. Maksimcuka, P. J. Withers and S. H. Cartmell, *BMC Biol.*, 2020, **18**, 21.
14 A. Sun, X. Liu and G. Tang, *Front. Chem.*, 2017, **5**, 124.
15 W. Liu, J. Chen and Z. Xu, *Coord. Chem. Rev.*, 2021, **429**, 213638.
16 N. Kwon, D. Kim, K. M. K. Swamy and J. Yoon, *Coord. Chem. Rev.*, 2021, **427**, 213581.
17 A.-M. Caminade, A. Hameau, C.-O. Turrin, R. Laurent and J.-P. Majoral, *Coord. Chem. Rev.*, 2021, **430**, 213739.
18 D. L. Ma, C. Wu, G. Li, T. L. Yung and C. H. Leung, *J. Mater. Chem. B*, 2020, **8**, 4715–4725.
19 Y. Ning, G. Q. Jin, M. X. Wang, S. Gao and J. L. Zhang, *Curr. Opin. Chem. Biol.*, 2022, **66**, 102097.
20 S. Nasiri Sovari and F. Zobi, *Chemistry*, 2020, **2**, 418–452.
21 D. A. Iovan, S. Jia and C. J. Chang, *Inorg. Chem.*, 2019, **58**, 13546–13560.
22 Y. Lu, N. Yeung, N. Sieracki and N. M. Marshall, *Nature*, 2009, **460**, 855–862.

23 C. Glorieux and P. B. Calderon, *Biol. Chem.*, 2017, **398**, 1095–1108.
24 S. Yoshikawa and A. Shimada, *Chem. Rev.*, 2015, **115**, 1936–1989.
25 G. R. Warner, Y. Somasundar, K. C. Jansen, E. Z. Kaaret, C. Weng, A. E. Burton, M. R. Mills, L. Q. Shen, A. D. Ryabov, G. Pros, T. Pintauer, S. Biswas, M. P. Hendrich, J. A. Taylor, F. S. Vom Saal and T. J. Collins, *ACS Catal.*, 2019, **9**, 7023–7037.
26 E. Kuah, S. Toh, J. Yee, Q. Ma and Z. Gao, *Chem.–Eur. J.*, 2016, **22**, 8404–8430.
27 C. Wang, N. Zhang, C.-Y. Hou, X.-X. Han, C.-H. Liu, Y.-H. Xing, F.-Y. Bai and L.-X. Sun, *Transition Met. Chem.*, 2020, **45**, 423–433.
28 K. J. Bruemmer, S. W. M. Crossley and C. J. Chang, *Angew. Chem., Int. Ed.*, 2020, **59**, 13734–13762.
29 H. Singh, K. Tiwari, R. Tiwari, S. K. Pramanik and A. Das, *Chem. Rev.*, 2019, **119**, 11718–11760.
30 N. Kumar, Roopa, V. Bhalla and M. Kumar, *Coord. Chem. Rev.*, 2021, **427**, 213550.
31 R. Botár, E. Molnár, Z. Garda, E. Madarasi, G. Trencsényi, J. Kiss, F. K. Kálmán and G. Tircsó, *Inorg. Chem. Front.*, 2022, **9**, 577–583.
32 A. Sinopoli, N. T. La Porte, J. F. Martinez, M. R. Wasielewski and M. Sohail, *Coord. Chem. Rev.*, 2018, **365**, 60–74.
33 J. Berrones Reyes, M. K. Kuimova and R. Vilar, *Curr. Opin. Chem. Biol.*, 2021, **61**, 179–190.
34 D. Parker, J. D. Fradgley and K. L. Wong, *Chem. Soc. Rev.*, 2021, **50**, 8193–8213.
35 V. A. Larson, B. Battistella, K. Ray, N. Lehnert and W. Nam, *Nat. Rev. Chem.*, 2020, **4**, 404–419.
36 J. A. Drewry and P. T. Gunning, *Coord. Chem. Rev.*, 2011, **255**, 459–472.
37 H. Li, D. Kim, Q. Yao, H. Ge, J. Chung, J. Fan, J. Wang, X. Peng and J. Yoon, *Angew. Chem., Int. Ed.*, 2021, **60**, 17268–17289.
38 H. Xiao, W. Zhang, P. Li, W. Zhang, X. Wang and B. Tang, *Angew. Chem., Int. Ed.*, 2019, **59**, 4216–4230.
39 A. C. Sedgwick, L. Wu, H. H. Han, S. D. Bull, X. P. He, T. D. James, J. L. Sessler, B. Z. Tang, H. Tian and J. Yoon, *Chem. Soc. Rev.*, 2018, **47**, 8842–8880.
40 A. Vogler and H. Kunkely, *Luminescent Metal Complexes: Diversity of Excited States*, Springer, Berlin, 2001.
41 Y. Y. Chia and M. G. Tay, *Dalton Trans.*, 2014, **43**, 13159–13168.
42 M. D. Allendorf, C. A. Bauer, R. K. Bhakta and R. J. Houk, *Chem. Soc. Rev.*, 2009, **38**, 1330–1352.
43 M. L. Aulsebrook, B. Graham, M. R. Grace and K. L. Tuck, *Coord. Chem. Rev.*, 2018, **375**, 191–220.
44 X. Zhen, R. Qu, W. Chen, W. Wu and X. Jiang, *Biomater. Sci.*, 2021, **9**, 285–300.
45 D. Wu, L. Chen, Q. Xu, X. Chen and J. Yoon, *Acc. Chem. Res.*, 2019, **52**, 2158–2168.
46 A. S. M. Islam, M. Sasmal, D. Maiti, A. Dutta, S. Ganguly, A. Katarkar, S. Gangopadhyay and M. Ali, *ACS Appl. Bio Mater.*, 2019, **2**, 1944–1955.
47 Y. Gou, M. Chen, S. Li, J. Deng, J. Li, G. Fang, F. Yang and G. Huang, *J. Med. Chem.*, 2021, **64**, 5485–5499.
48 H. Wang, V. C. Jordan, I. A. Ramsay, M. Sojoodi, B. C. Fuchs, K. K. Tanabe, P. Caravan and E. M. Gale, *J. Am. Chem. Soc.*, 2019, **141**, 5916–5925.
49 K. Du, E. A. Waters and T. D. Harris, *Chem. Sci.*, 2017, **8**, 4424–4430.
50 G. S. Loving, S. Mukherjee and P. Caravan, *J. Am. Chem. Soc.*, 2013, **135**, 4620–4623.
51 M. Yu, B. S. Bouley, D. Xie and E. L. Que, *Dalton Trans.*, 2019, **48**, 9337–9341.
52 J. Ruiz-Cabello, B. P. Barnett, P. A. Bottomley and J. W. Bulte, *NMR Biomed.*, 2011, **24**, 114–129.
53 K. L. Peterson, K. Srivastava and V. C. Pierre, *Front. Chem.*, 2018, **6**, 160.
54 P. C. M. van Zijl and N. N. Yadav, *Magn. Reson. Med.*, 2011, **65**, 927–948.
55 E. Terreno, D. D. Castelli, A. Viale and S. Aime, *Chem. Rev.*, 2010, **110**, 3019–3042.
56 S. Zhang, M. Merritt, D. E. Woessner, R. E. Lenkinski and A. D. Sherry, *Acc. Chem. Res.*, 2003, **36**, 783–790.
57 J. H. McCullough, *Evol. Med. Public Health*, 2015, **2015**, 149.
58 J. Wade, D. J. Byrne, C. J. Ballentine and H. Drakesmith, *Proc. Natl. Acad. Sci. U. S. A.*, 2021, **118**, e2109865118.
59 T. Ganz and E. Nemeth, *Nat. Rev. Immunol.*, 2015, **15**, 500–510.
60 K. D. Dubey and S. Shaik, *Acc. Chem. Res.*, 2019, **52**, 389–399.
61 B. C. Bales, B. Grimmond, B. F. Johnson, M. T. Luttrell, D. E. Meyer, T. Polyanskaya, M. J. Rishel and J. Roberts, *Contrast Media Mol. Imaging*, 2019, **2019**, 8356931.
62 P. Papan, J. Kantapan, P. Sangthong, P. Meepowpan and N. Dechsupa, *Contrast Media Mol. Imaging*, 2020, **2020**, 8877862.
63 M. Y. Lee, D. Choi, M. S. Jang and J. H. Lee, *Bioconjugate Chem.*, 2018, **29**, 2426–2435.
64 D. Asik, S. M. Abozeid, S. G. Turowski, J. A. Spernyak and J. R. Morrow, *Inorg. Chem.*, 2021, **60**, 8651–8664.
65 L. Palagi, E. Di Gregorio, D. Costanzo, R. Stefania, C. Cavallotti, M. Capozza, S. Aime and E. Gianolio, *J. Am. Chem. Soc.*, 2021, **143**, 14178–14188.
66 E. M. Snyder, D. Asik, S. M. Abozeid, A. Burgio, G. Bateman, S. G. Turowski, J. A. Spernyak and J. R. Morrow, *Angew. Chem., Int. Ed.*, 2020, **59**, 2414–2419.
67 A. Patel, D. Asik, J. A. Spernyak, P. J. Cullen and J. R. Morrow, *J. Inorg. Biochem.*, 2019, **201**, 110832.
68 C. Das, A. Mondal, S. Sengupta, C. Cardin and S. K. Chattopadhyay, *Spectrochim. Acta, Part A*, 2022, **273**, 120943.
69 P. B. Tsitovich, F. Gendron, A. Y. Nazarenko, B. N. Livesay, A. P. Lopez, M. P. Shores, J. Autschbach and J. R. Morrow, *Inorg. Chem.*, 2018, **57**, 8364–8374.
70 S. M. Abozeid, M. S. I. Chowdhury, D. Asik, J. A. Spernyak and J. R. Morrow, *ACS Appl. Bio Mater.*, 2021, **4**, 7951–7960.
71 D. Asik, R. Smolinski, S. M. Abozeid, T. B. Mitchell, S. G. Turowski, J. A. Spernyak and J. R. Morrow, *Molecules*, 2020, **25**, 2291.

72 L. An, Y. Cai, Q. Tian, J. Lin and S. Yang, *Sci. China Mater.*, 2020, **64**, 498–509.
73 K. Srivastava, G. Ferrauto, V. G. Young, Jr, S. Aime and V. C. Pierre, *Inorg. Chem.*, 2017, **56**, 12206–12213.
74 H. Wang, A. Wong, L. C. Lewis, G. R. Nemeth, V. C. Jordan, J. W. Bacon, P. Caravan, H. S. Shafaat and E. M. Gale, *Inorg. Chem.*, 2020, **59**, 17712–17721.
75 S. Shankar, M. Peters, K. Steinborn, B. Krahwinkel, F. D. Sonnichsen, D. Grote, W. Sander, T. Lohmiller, O. Rudiger and R. Herges, *Nat. Commun.*, 2018, **9**, 4750.
76 M. K. Peters, S. Hamer, T. Jakel, F. Rohricht, F. D. Sonnichsen, C. von Essen, M. Lahtinen, C. Naether, K. Rissanen and R. Herges, *Inorg. Chem.*, 2019, **58**, 5265–5272.
77 J. Salaam, M. Rivat, T. Fogeron and J. Hasserodt, *Analysis & Sensing*, 2020, **1**, 11–29.
78 F. Touti, P. Maurin and J. Hasserodt, *Angew. Chem., Int. Ed.*, 2013, **52**, 4654–4658.
79 F. Touti, A. K. Singh, P. Maurin, L. Canaple, O. Beuf, J. Samarut and J. Hasserodt, *J. Med. Chem.*, 2011, **54**, 4274–4278.
80 D. Maheshwaran, T. Nagendraraj, T. Sekar Balaji, G. Kumaresan, S. Senthil Kumaran and R. Mayilmurugan, *Dalton Trans.*, 2020, **49**, 14680–14689.
81 P. Xiang, Y. Shen, J. Shen, Z. Feng, M. Sun, Q. Zhang, S. Li, D. Li, G. Zhang, Z. Wu, Y. Tian, Z. Zhang and X. Tian, *Inorg. Chem. Front.*, 2020, **7**, 2753–2758.
82 V. C. Culotta and M. J. Daly, *Antioxid. Redox Signaling*, 2013, **19**, 933–944.
83 D. K. Dogutan and D. G. Nocera, *Acc. Chem. Res.*, 2019, **52**, 3143–3148.
84 D. Ndiaye, M. Sy, A. Pallier, S. Meme, I. de Silva, S. Lacerda, A. M. Nonat, L. J. Charbonniere and É. Tóth, *Angew. Chem., Int. Ed.*, 2020, **59**, 11958–11963.
85 M. Devreux, C. Henoumont, F. Dioury, S. Boutry, O. Vacher, L. V. Elst, M. Port, R. N. Muller, O. Sandre and S. Laurent, *Inorg. Chem.*, 2021, **60**, 3604–3619.
86 B. Phukan, C. Mukherjee, U. Goswami, A. Sarmah, S. Mukherjee, S. K. Sahoo and S. C. Moi, *Inorg. Chem.*, 2018, **57**, 2631–2638.
87 K. Chen, P. Li, C. Zhu, Z. Xia, Q. Xia, L. Zhong, B. Xiao, T. Cheng, C. Wu, C. Shen, X. Zhang and J. Zhu, *J. Med. Chem.*, 2021, **64**, 9182–9192.
88 M. K. Islam, S. Kim, H. K. Kim, S. Park, G. H. Lee, H. J. Kang, J. C. Jung, J. S. Park, T. J. Kim and Y. Chang, *J. Med. Chem.*, 2017, **60**, 2993–3001.
89 J. Wang, H. Wang, I. A. Ramsay, D. J. Erstad, B. C. Fuchs, K. K. Tanabe, P. Caravan and E. M. Gale, *J. Med. Chem.*, 2018, **61**, 8811–8824.
90 D. Lalli, G. Ferrauto, E. Terreno, F. Carniato and M. Botta, *J. Mater. Chem. B*, 2021, **9**, 8994–9004.
91 R. Botar, E. Molnar, G. Trencsenyi, J. Kiss, F. K. Kalman and G. Tircsó, *J. Am. Chem. Soc.*, 2020, **142**, 1662–1666.
92 R. Uzal-Varela, A. Rodriguez-Rodriguez, M. Martinez-Calvo, F. Carniato, D. Lalli, D. Esteban-Gomez, I. Brandariz, P. Perez-Lourido, M. Botta and C. Platas-Iglesias, *Inorg. Chem.*, 2020, **59**, 14306–14317.
93 S. Chirayil, V. C. Jordan, A. F. Martins, N. Paranawithana, S. J. Ratnakar and A. D. Sherry, *Inorg. Chem.*, 2021, **60**, 2168–2177.
94 A. Barandov, B. B. Bartelle, C. G. Williamson, E. S. Loucks, S. J. Lippard and A. Jasanoff, *Nat. Commun.*, 2019, **10**, 897.
95 F. K. Kalman, V. Nagy, B. Varadi, Z. Garda, E. Molnar, G. Trencsenyi, J. Kiss, S. Meme, W. Meme, É. Tóth and G. Tircsó, *J. Med. Chem.*, 2020, **63**, 6057–6065.
96 A. Forgacs, L. Tei, Z. Baranyai, D. Esteban-Gomez, C. Platas-Iglesias and M. Botta, *Dalton Trans.*, 2017, **46**, 8494–8504.
97 S. Anbu, S. H. L. Hoffmann, F. Carniato, L. Kenning, T. W. Price, T. J. Prior, M. Botta, A. F. Martins and G. J. Stasiuk, *Angew. Chem., Int. Ed.*, 2021, **60**, 10736–10744.
98 G. Rolla, V. De Biasio, G. B. Giovenzana, M. Botta and L. Tei, *Dalton Trans.*, 2018, **47**, 10660–10670.
99 G. S. Loving, S. Mukherjee and P. Caravan, *J. Am. Chem. Soc.*, 2013, **135**, 4620–4623.
100 T. E. Hutchinson, A. Bashir, M. Yu, R. J. Beyers and C. R. Goldsmith, *Inorg. Chim. Acta*, 2019, **496**, 119045.
101 M. Yu, M. B. Ward, A. Franke, S. L. Ambrose, Z. L. Whaley, T. M. Bradford, J. D. Gorden, R. J. Beyers, R. C. Cattley, I. Ivanovic-Burmazovic, D. D. Schwartz and C. R. Goldsmith, *Inorg. Chem.*, 2017, **56**, 2812–2826.
102 H. Chen, X. Tang, X. Gong, D. Chen, A. Li, C. Sun, H. Lin and J. Gao, *Chem. Commun.*, 2020, **56**, 4106–4109.
103 S. M. A. Pinto, M. J. F. Calvete, M. E. Ghica, S. Soler, I. Gallardo, A. Pallier, M. B. Laranjo, A. M. S. Cardoso, M. Castro, C. M. A. Brett, M. M. Pereira, É. Tóth and C. Geraldes, *Dalton Trans.*, 2019, **48**, 3249–3262.
104 Y. Ren, A. C. Sedgwick, J. Chen, G. Thiabaud, C. V. Chau, J. An, J. F. Arambula, X. P. He, J. S. Kim, J. L. Sessler and C. Liu, *J. Am. Chem. Soc.*, 2020, **142**, 16156–16160.
105 X. Tian, L. Xiao, Y. Shen, L. Luo, G. Zhang, Q. Zhang, D. Li, J. Wu, Z. Wu, Z. Zhang and Y. Tian, *Inorg. Chem. Front.*, 2019, **6**, 2914–2920.
106 M. K. Tiwari, P. M. Hagglund, I. M. Moller, M. J. Davies and M. J. Bjerrum, *Redox Biol.*, 2019, **26**, 101262.
107 R. Memary, D. Giurco, G. Mudd and L. Mason, *J. Cleaner Prod.*, 2012, **33**, 97–108.
108 S. Mahata, S. Dey, B. B. Mandal and V. Manivannan, *J. Photochem. Photobiol., A*, 2022, **427**, 113795.
109 X. Shang, X. Yue, Y. Chen, C. Li, H. Chen and T. Wang, *Inorg. Chem. Commun.*, 2019, **99**, 1–10.
110 S. Khanra, S. Ta, A. Paladhi, M. Ghosh, S. Ghosh, S. K. Hira, P. P. Manna, P. Brandao, V. Felix and D. Das, *Chem. Commun.*, 2020, **56**, 6563–6566.
111 J. Li, L. Wang, Z. Zhao, X. Li, X. Yu, P. Huo, Q. Jin, Z. Liu, Z. Bian and C. Huang, *Angew. Chem., Int. Ed.*, 2020, **59**, 8210–8217.
112 L. Lei, W. Xie, Z. Chen, Y. Jiang and Y. Liu, *Sens. Actuators, B*, 2018, **273**, 35–40.
113 D. Zhang, X. Mao, Z. Zhang, S. Zhang, J. Chen, D. Shan and X. Lu, *Sens. Actuators, B*, 2019, **284**, 684–694.
114 D. Maiti, A. S. M. Islam, A. Dutta, M. Sasmal, C. Prodhan and M. Ali, *Dalton Trans.*, 2019, **48**, 2760–2771.
115 A. Loas and S. J. Lippard, *J. Mater. Chem. B*, 2017, **5**, 8929–8933.

116 D. Maheshwaran, S. Priyanga and R. Mayilmurugan, *Dalton Trans.*, 2017, **46**, 11408–11417.
117 S. Priyanga, T. Khamrang, M. Velusamy, S. Karthi, B. Ashokkumar and R. Mayilmurugan, *Dalton Trans.*, 2019, **48**, 1489–1503.
118 Y.-H. Deng, R.-Y. Li, J.-Q. Zhang, Y.-F. Wang, J.-T. Li, W.-T. Guo and W.-K. Dong, *New J. Chem.*, 2021, **45**, 8597–8607.
119 D. Chao and Y. Zhang, *Sens. Actuators, B*, 2017, **245**, 146–155.
120 S. N. Yin, Y. Liu, C. Zhou and S. Yang, *Nanomater*, 2017, **7**, 132.
121 J. S. Enriquez, M. Yu, B. S. Bouley, D. Xie and E. L. Que, *Dalton Trans.*, 2018, **47**, 15024–15030.
122 R. T. Kadakia, D. Xie, D. Martinez, M. Yu and E. L. Que, *Chem. Commun.*, 2019, **55**, 8860–8863.
123 K. E. Prosser, D. Xie, A. Chu, G. A. MacNeil, B. R. Varju, R. T. Kadakia, E. L. Que and C. J. Walsby, *Chem.–Eur. J.*, 2021, **27**, 9839–9849.
124 D. Xie, S. Kim, V. Kohli, A. Banerjee, M. Yu, J. S. Enriquez, J. J. Luci and E. L. Que, *Inorg. Chem.*, 2017, **56**, 6429–6437.
125 M. A. Akl, E. R. El-Gharkawy, N. A. El-Mahdy, S. M. El-Sheikh and S. M. Sheta, *Dalton Trans.*, 2020, **49**, 15769–15778.
126 A. Bhattacharyya, A. Jameei, A. Garai, R. Saha, A. A. Karande and A. R. Chakravarty, *Dalton Trans.*, 2018, **47**, 5019–5030.
127 C. Vidya Rani, M. P. Kesavan, S. Haseena, R. Varatharaj, J. Rajesh and G. Rajagopal, *Appl. Biochem. Biotechnol.*, 2020, **191**, 1515–1532.